A Correction for the Thermal Mass–Induced Errors of CTD Tags Mounted on Marine Mammals

Vigan Mensah, Fabien Roquet, Lia Siegelman-Charbit, Baptiste Picard, Etienne Pauthenet, Christophe Guinet

A Correction for the Thermal Mass–Induced Errors of CTD Tags Mounted on Marine Mammals

VIGAN MENSAH,[a] FABIEN ROQUET,[b,c] LIA SIEGELMAN-CHARBIT,[d,e], BAPTISTE PICARD,[f] ETIENNE PAUTHENET,[b] AND CHRISTOPHE GUINET[f]

[a] *Institute of Low Temperature Science, Hokkaido University, Sapporo, Japan*
[b] *Department of Meteorology (MISU), Stockholm University, Stockholm, Sweden*
[c] *Department of Marine Sciences, University of Gothenburg, Gothenburg, Sweden*
[d] *Marine Environmental Science Laboratory (LEMAR), Plouzane, France*
[e] *Laboratory for Ocean Physics and Satellite Remote Sensing (LOPS), Plouzane, France*
[f] *Centre d'Etudes Biologiques de Chizé (CNRS), Villiers-en-Bois, France*

(Manuscript received 24 August 2017, in final form 31 March 2018)

ABSTRACT

The effect of thermal mass on the salinity estimate from conductivity–temperature–depth (CTD) tags sensor mounted on marine mammals is documented, and a correction scheme is proposed to mitigate its impact. The algorithm developed here allows for a direct correction of the salinity data, rather than a correction of the sample's conductivity and temperature. The amplitude of the thermal mass–induced error on salinity and its correction are evaluated via comparison between data from CTD tags and from Sea-Bird Scientific CTD used as a reference. Thermal mass error on salinity appears to be generally $O(10^{-2})$ g kg^{-1}, it may reach $O(10^{-1})$ g kg^{-1}, and it tends to increase together with the magnitude of the cumulated temperature gradient (T_{HP}) within the water column. The correction we propose yields an error decrease of up to ~60% if correction coefficients specific to a certain tag or environment are calculated, and up to 50% if a default value for the coefficients is provided. The correction with the default coefficients was also evaluated using over 22 000 in situ dive data from five tags deployed in the Southern Ocean and is found to yield significant and systematic improvements on the salinity data, including for profiles whose T_{HP} was weak and the error small. The correction proposed here yields substantial improvements in the density estimates, although a thermal mass–induced error in temperature measurements exists for very large T_{HP} and has yet to be corrected.

1. Introduction

The Conductivity–Temperature–Depth Satellite Relay Data Logger (CTD-SRDL) tags (referred as "tag" in the following), developed at the Sea Mammal Research Unit (SMRU; University of St. Andrews, United Kingdom), are routinely deployed on various species of seals, such as southern elephant seals, *Mirounga leonina*; Steller sea lions, *Eumetopias jubatus*; or ribbon seals, *Histriophoca fasciat*. They represent a tremendous source of hydrographic data in largely undersampled areas, such as the Southern Ocean or the northern subpolar regions (Roquet et al. 2014; Treasure et al. 2017; see http://meop.net for more information). The temperature and conductivity sensors fitted on tags, manufactured by Valeport Ltd. (Totnes, United Kingdom), yield high precision (±0.005 for temperature and ±0.01 ms cm^{-1} for conductivity; see Boehme et al. 2009) and reasonable accuracies (±0.02°C for temperature and ±0.03 psu for salinity) after delayed-mode calibration (Roquet et al. 2011). However, a recent study by Nakanowatari et al. (2017) demonstrated that the tags are also affected by a thermal mass error—a phenomenon resulting from the transfer of heat from the sensor's walls to the sample being measured—on both their temperature and conductivity cells. Salinity being estimated via measurements of conductivity and temperature, the error in these measurements reflects on the salinity estimates, which display large discrepancies across sharp thermoclines.

Denotes content that is immediately available upon publication as open access.

Corresponding author: V. Mensah, vmensah@lowtem.hokudai.ac.jp

DOI: 10.1175/JTECH-D-17-0141.1

The thermal mass phenomenon and its effect on salinity data have been well documented for the Sea-Bird Scientific SBE4 conductivity sensor (Lueck 1990), and they manifest in areas of large temperature gradients, such as the seasonal thermocline, where large salinity spikes of $O(10^{-2})$–$O(10^{-1})$ psu appear, followed by a slow decaying hysteresis. A correction model has been developed by Lueck and Picklo (1990), and adjustments to the correction coefficients have subsequently been implemented by Morison et al. (1994), Mensah et al. (2009), Garau et al. (2011), and Liu et al. (2015). Nakanowatari et al. (2017) successfully applied the correction method on a set of eight tags deployed on seals in the Okhotsk Sea between 2011 and 2014, proposing a set of correction coefficients validated by comparing corrected salinity results with spatially and temporally averaged historical data. However, the effectiveness of this correction methodology in various oceanic conditions and geographical locations merits further assessment.

In this paper we first document the effects of thermal mass error on tag data by comparing results of temperature, conductivity, and salinity profiles obtained simultaneously by tags and by SBE CTDs attached together on the same frame. We then develop and implement a thermal mass correction model loosely based on Lueck and Picklo (1990)—but applied directly to the salinity data—and we estimate its effectiveness on our comparison dataset. The data tested for this study having been sampled under various hydrographic and thermocline conditions, we can therefore correct each tag's data with two different sets of correction coefficients: 1) a set of coefficients optimized for each specific tag sensor and 2) a unique set of coefficients (called generic coefficients) valid for any tag sensors and in any oceanic condition. The current study builds on Nakanowatari et al. (2017), proposing a comprehensive assessment of the effects of thermal mass error on CTD-SRDL tag measurements, and introduces a generic method to optimally reduce thermal mass–induced errors.

The thermal mass error affecting the tags and the salinity correction method are introduced in section 2. Section 3 presents the implementation of the correction scheme and a comparison of corrected tags' data versus reference CTD data, as well as a discussion on the effect of the correction obtained with the optimized and generic sets of correction coefficients. The generic coefficients are further tested on tens of thousands of in situ profiles in the Southern Ocean using upcast and downcast data as a mean of comparison, and these results are presented in section 4. A summary and conclusions are proposed in section 5.

2. Thermal mass–induced errors and its correction for CTD and tag sensors

a. Theory

The thermal mass is a well-known phenomenon that affects primarily the conductivity cells of various CTD sensors, especially when the cell is unpumped as is the case for the tags. Inductive conductivity cells are made of a cylinder through which the water flows as the CTD conducts its profile. Depending on the constructor, the cell is made of glass or ceramic and is typically surrounded by a layer of epoxy for protection. During profiling, the heat capacity of the sensor's walls and protective layer causes heat to be stored within the sensor. This heat or "thermal mass" is exchanged through the sensor's walls, thus contaminating the temperature—and hence the conductivity—of the water sample. While the temperature is accurately measured by the separate CTD temperature sensor, the sample's conductivity is modified because of the thermal mass, which yields a significant discrepancy in the salinity estimation. This error has been observed on the Sea-Bird Scientific SBE4 conductivity cell, which is part of the SBE9 CTD system, and depends on the temperature gradient (function of depth or time). It is particularly evident in situations of sharp thermocline (Lueck and Picklo 1990; Morison et al. 1994; Mensah et al. 2009; Liu et al. 2015). This issue has been addressed in several works, with a thermal correction model developed by Lueck (1990) specifically for the SBE sensor. In that study the thermal mass error is modeled as an error amplitude α_C, decaying within a relaxation time $1/\beta$ (Lueck 1990). The conductivity is then corrected via

$$C_T(n) = \Gamma_C \alpha_C (1 - 0.5\beta\Delta_t)^{-1} T_{\mathrm{HP}}(n), \qquad (1)$$

where C_T is the correction of conductivity added to the conductivity of the nth sample; $T_{\mathrm{HP}}(n)$ is the high-pass filtered sample's temperature [see Eq. (A4)], using a first-order discrete-time filter with a time constant $\tau = \beta^{-1} - 0.5\Delta_t$; n is the sample index; $\Gamma_C = \partial C/\partial T_{S,p}$ is the coefficient of sensitivity of conductivity to temperature; and Δ_t is the sampling time interval. This model has been successfully implemented with various sets of α_C and β coefficients for the SBE4. In the limit case $\Delta_t\beta \ll 1$ (i.e., when the response time is much larger than the sampling interval), the correction simply becomes $C_T = \Gamma_C \alpha_C T_{\mathrm{HP}}$ with a time constant $= \beta^{-1}$. Note that the formulation of the correction given here differs from the one given in Lueck and Picklo (1990); however, both are formally equivalent as shown in the appendix. The formulation given here is preferred because it is more readily interpretable in terms of a standard discrete-time high-pass filter.

The setting and technology of the tag sensor differ from those of the SBE4 cell, in that the wall of the conductivity sensor is made of ceramic for the tag instead of glass for the CTD cell, and the latter is an electrode cell, whereas the tag cell is inductive. Despite these differences in design, the tags are likely to show similar signs of thermal mass–induced anomalies as a result of the water sample passing through a few centimeters of long pipe, itself covered by epoxy resin. The thickness of the epoxy layer is sensibly larger than on the SBE4 cell and, should the tag sensor indeed be affected by a thermal mass error, longer relaxation time than for the SBE cell are expected. Importantly, with the platinum resistance temperature sensor being located in the immediate vicinity upstream of the conductivity cell and surrounded by epoxy, a thermal mass error may also affect the temperature measurements, contrary to the SBE CTD.

Following Morison et al. (1994), temperature could be corrected with a similar scheme as conductivity according to

$$T_T(n) = \alpha_T(1 - 0.5\beta\Delta_t)^{-1} T_{\mathrm{HP}}(n), \qquad (2)$$

where the only formal difference with (1) is that no sensitivity coefficient is required in the case of a temperature correction.

b. *Illustration of the thermal mass error on tag data*

To assess the possibility of a thermal mass error affecting both the tags' temperature and conductivity sensors, we tested the response of four tags to high-temperature gradients in in situ situations. As part of the Bouée pour l'acquisition de Séries Optiques à Long Terme (BOUSSOLE) program (Antoine et al. 2006, 2008) in the Ligurian Sea, the four sensors were attached together with an SBE9 CTD system, which is used as a reference, and seven casts were conducted. Each tag's temperature, conductivity, and salinity profile is corrected for bias and pressure-induced slope following Roquet et al. (2011). The test was conducted at the BOUSSOLE mooring site (43°20′N, 7°54′E) in the northwestern Mediterranean Sea, on board the Sailing School Vessel (SSV) *Tethys II*. The experiment was carried out on 11 and 12 June 2008, during which a seasonal thermocline of gradient ~0.2°C m^{-1} occurred between ~10- and ~50-m depth, and with local maximum gradient of ~0.6°C m^{-1}. Our test is therefore suited for detecting and characterizing errors in a nearly idealized, steplike environment, as it was done in Lueck and Picklo (1990), Morison et al. (1994), and Mensah et al. (2009). The results of this experiment are illustrated in Fig. 1, where profiles of temperature, conductivity, and salinity (Figs. 1a–c) are plotted for both CTD and tags, whereas the difference between the sensors are plotted in Figs. 1d–f. The presence of thermal mass–induced error is highlighted by the 30-m low-pass filtered curves (green lines) in Figs. 1d–f. Strong anomalies exist for both the temperature and conductivity, with a low-frequency error $O(10^{-1})$°C and (10^{-2}) ms cm^{-1} for temperature (Fig. 1d) and conductivity (Fig. 1e), respectively. These errors reflect on the salinity estimation, yielding a maximum error $O(10^{-1})$ psu (green line in Fig. 1f). While the scale of the temperature error will be shown to be exceptional as a result of the extreme magnitude of the temperature gradient, the order of magnitude for the conductivity error is usual for temperature gradients greater than 0.1°C m^{-1} (section 3). Also, the rather extreme temperature gradients observed in this experiment are not unusual in some of the regions sampled by the marine mammals carrying the tags, such as the Okhotsk Sea (Nakanowatari et al. 2017).

Besides the typically large-scaled and long-term thermal mass error, discrepancies of smaller scale and shorter term are evidenced from the profiles of conductivity difference (Fig. 1e) and temperature difference (Fig. 1d). These errors do not show clearly on the profiles of temperature and conductivity but manifest on the salinity profile (Fig. 1c) as spikes of $O(10^{-2})$ psu. Such high-frequency error may be caused by the irregular flow within the tag sensors; as contrary to the SBE4 cell, the tag is not fitted with a pump to stabilize the inflow. In contrast with the terminology used in the rest of this paper, salinity results in Fig. 1 are expressed in practical salinity units [practical salinity scale 1978 (PSS-78) to illustrate the direct link between conductivity measurement and salinity estimate. However, in the following chapters, all salinity results in the tables, text, and figures will be expressed as Absolute Salinity (g kg^{-1}) in order to follow the new standard recommendations (McDougall et al. 2012). While the values in an Absolute Salinity profile are generally shifted by ~0.16 compared to those of a practical salinity profile, our correction scheme yields nearly identical results whether conducted on practical or Absolute Salinity profiles.

c. *An independent correction scheme for salinity*

As a preliminary test, both the conductivity and temperature profiles of each of the four tags were corrected using (1) and (2), respectively, with the arbitrary values $\alpha_C = 0.05$, $\alpha_T = 0.037$, and $\beta = 1/30$ s^{-1}. This test produced a significant reduction of the error (not shown) in the temperature, conductivity, and salinity data of profiles such as the one displayed in Fig. 1.

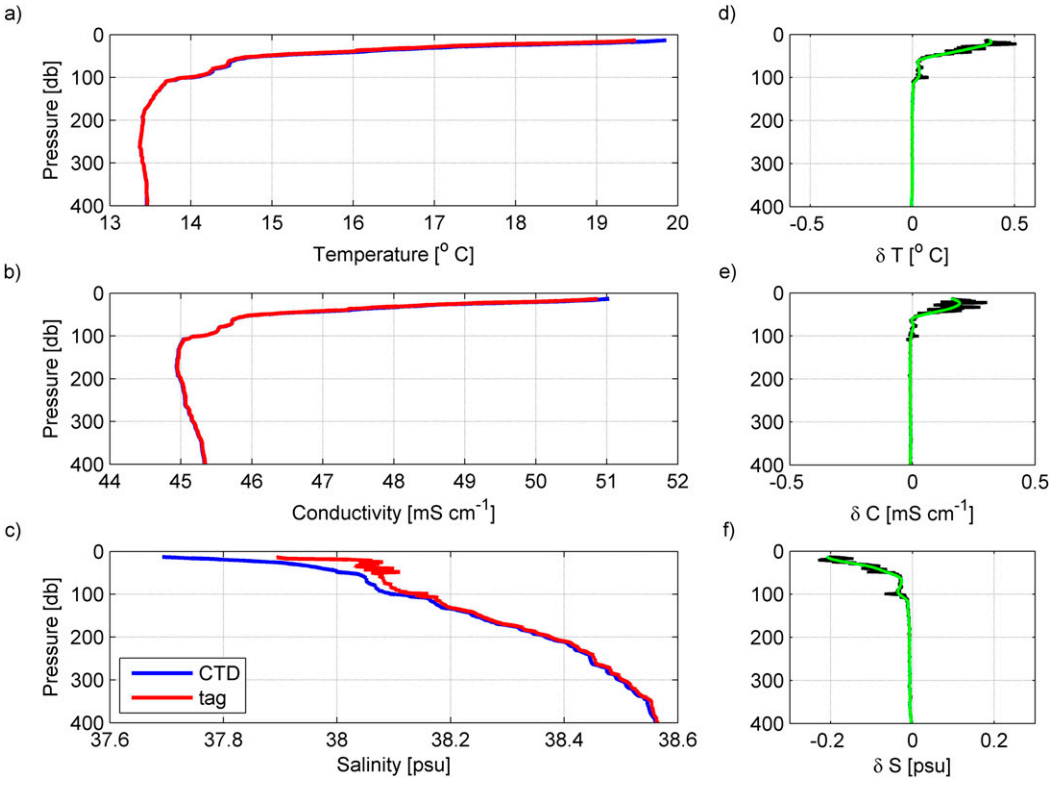

FIG. 1. CTD-SRDL and reference SBE CTD cast acquired on 11 Jun 2008 at the BOUSSOLE mooring site. (a) Temperature profiles, (b) conductivity, and (c) salinity. (d) Temperature, (e) conductivity, and (f) salinity difference (CTD minus tag) between both sensors, respectively. The 30-m low-passed filter signal is shown in (d)–(f) (green line). The thermal mass error is characterized by the strong, low-frequency anomaly visible above the thermocline within the upper 50 m.

However, correcting the temperature and conductivity separately may lead to some ambiguity in the correction of the salinity estimate. Residual discrepancies may remain as a result of various causes—for example, a misestimate of the coefficient values for the thermal mass correction or a slight misalignment of the CTD and tag pressures—making it possible for the temperature and conductivity residual errors to compensate each other and to yield a correct salinity estimate. Thus, the search for optimal correction coefficients for temperature and conductivity would be hampered by such considerations. Also, the error in salinity of $O(10^{-2})$–$O(10^{-1})$ g kg^{-1} is generally between one order below and the same order of magnitude as the salinity variations within any given cast. In contrast, the temperature error is most often of $O(10^{-2})$°C, which is two to three orders of magnitude below the typical variations observed within one profile, making the error signal less evident to detect and to correct following the methods described in the next section.

For the sake of practicality, finding a way to correct the salinity estimate directly becomes necessary, and a correction scheme based on (1) could be implemented following the small-amplitude assumption that the salinity correction is a linear combination of the effect of conductivity and temperature corrections:

$$S_T = \frac{\partial S}{\partial C_{T,p}} C_T + \frac{\partial S}{\partial T_{C,p}} T_T. \tag{3}$$

As the causes of the temperature and conductivity thermal mass are similar, we may assume that the time constant β^{-1} that is included in the correction schemes (1) and (2) are identical, and we can establish the following salinity correction:

$$S_T(n) = \Gamma_S \alpha (1 - 0.5\beta\Delta_t)^{-1} T_{\mathrm{HP}}(n), \tag{4}$$

where $\Gamma_S = \partial S/\partial T_{C,p}$ is the coefficient of sensitivity of salinity to temperature, at fixed conductivity and pressure. The validity of (4) is ensured if within the range of salinity measured, the deviation of Γ_S is small. This is demonstrated in Fig. 2a and 2b, which display the values of Γ_C (coefficient of sensitivity of conductivity to temperature) and Γ_S at various values of temperature and

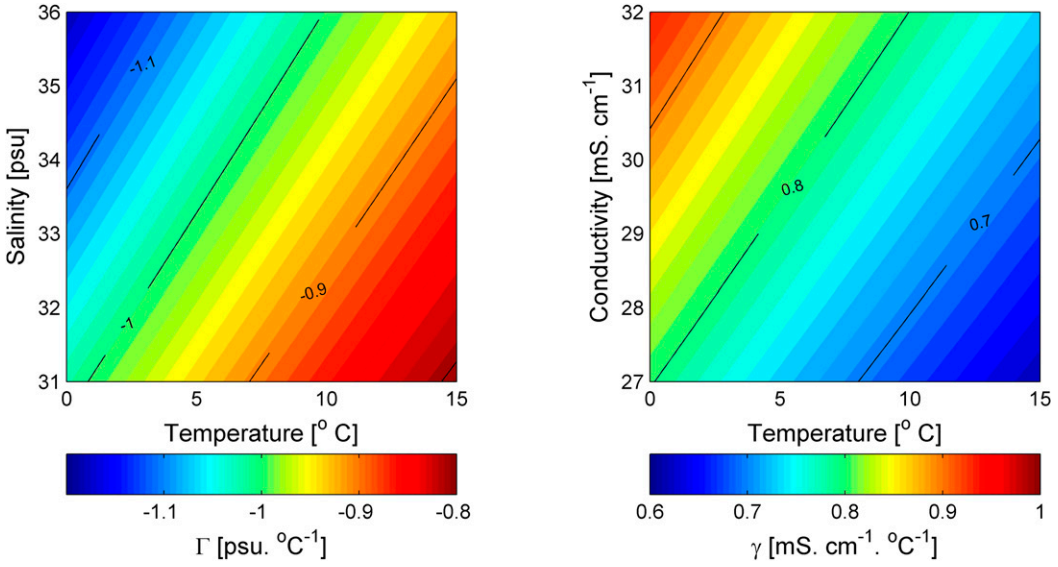

FIG. 2. Values of coefficients (a) Γ_S of sensitivity of salinity to temperature and (b) Γ_C of sensitivity of conductivity to temperature, for ranges of temperature and salinity (conductivity) typically measured in regions sampled by the tags.

conductivity (salinity), respectively. Applying temperature and conductivity corrections following (1) and (2) is equivalent to directly correcting salinity using (4) with an error magnitude $\alpha = \alpha_T - \alpha_C$. One major drawback of correcting directly salinity instead of temperature and conductivity separately, however, is that it might lead to uncorrected biases in both the temperature and density. The magnitude of residual density errors will be discussed later in the study.

3. Results

a. *Optimized correction coefficients*

1) DETERMINATION OF COEFFICIENTS

We collected data from six different calibration cruises, called ''experiments,'' during which a set of tags is attached to a CTD frame to conduct profiles simultaneously with an SBE9 CTD system, which is used as a reference. During each of the experiments, the tags were positioned upward (i.e., the temperature and conductivity sensors facing up) about 50–100 cm above the CTD, which was installed horizontally at the bottom of the CTD rosette. The profiles are compared during the upcast only, in order to match the in situ profiling conditions during which the tags are deployed over the head of marine mammals. One drawback in using upcast data, however, is that the CTD frame, being a source of turbulence, may generate minor discrepancies when comparing data acquired by tags and CTD. Both CTD and tags data are processed following their respective standard postprocessing procedures; the tags' temperature and conductivity sensors' pressure-dependent drifts were previously corrected via the method of Roquet et al. (2011). The root-mean-square (RMS) difference between the salinity obtained from the CTD and that obtained from the tags is called an error, and this is calculated before and after implementation of the correction scheme. The salinity correction delineated by (4) is tested through a least squares regression scheme, in which we look for the pair α_{opt}, β_{opt}, which minimizes the RMS error in salinity $F(\alpha, \beta)$, where

$$F(\alpha,\beta) = \sqrt{\frac{1}{N \times \text{nc}} \sum_{i=1}^{i=\text{nc}} \sum_{z=1}^{z=N} [S_{\text{ref}}(z,i) - S_{\text{tag}}^{\alpha,\beta}(z,i)]^2}. \quad (5)$$

The test was carried out separately for each of the n tags in order to obtain a set of optimum correction coefficient α and β; $z = 1,2,\ldots, N$ is the maximum depth of the measurement (dbar) and $i = 1, 2, \ldots,$ nc is the number of casts tested on a given tag. Prior to carrying out the least squares regression, all temperature and salinity profiles went through a low-pass filter with a cutoff value set at 10 m, thus avoiding the RMS difference to include high-frequency errors unrelated to thermal mass. During these six different experiments, a total of 113 profiles belonging to 42 tags were tested. Experiments Boussole08 and Boussole09 were conducted in the western Mediterranean Sea at the BOUSSOLE mooring location in June 2008 and November 2009, respectively. Both

of these experiments present strong thermoclines, where the time temperature gradient largely exceeds 0.1°C s^{-1} and where tag data are expected to exhibit strong signs of thermal mass errors. Experiment Carols08 was conducted in the Bay of Biscay in November 2008 and presents only a moderate thermocline as a result of the strong winds occurring in the eastern Atlantic in late autumn. Experiments Albion08 and Albion09 were conducted during the austral summer in the Dumont d'Urville Sea, off the coast of Adélie Land (Terre Adélie), Antarctica, and experiment iStar14 (https://www.istar.ac.uk/) occurred in the Amundsen Sea, Antarctica, in February 2014. The environment for the latter three experiments is characterized by water temperature between −1.8° and +2°C, and generally weaker temperature gradients than those encountered during the Mediterranean Sea or the Bay of Biscay experiments. Of these three experiments, iStar14 presents the largest gradients, with maximum values around 0.1°C s^{-1}. The values of the maximum temperature gradients (smoothed over a 10-m window) encountered during each of these experiments are indicated in Table 1. We also introduce in this table the value of the maximum high-passed temperature, T_{HP} [(1), (4)], which can be interpreted as the cumulated effect of the thermal mass on the conductivity sensor. In fact, the thermal mass effect may be more important for a profile where a weak temperature gradient is met by the sensors for a long time/distance than during a cast where a greater gradient occurs over a shorter time or distance. Therefore, T_{HP} enables the combined effect of the temperature gradient and its duration to be appropriately expressed. The variable T_{HP} depends on the value of β [section 2a and Eq. (A4)] and throughout this paper we calculate T_{HP} with $\beta = 0.060$ s^{-1}, this being the generic value found for coefficient β (section 3b).

2) Effects of the correction on salinity data

The value of optimum correction for each of the different experiments is indicated in Table 1, where the correction is defined as $D = F(0,0)_{\mathrm{MaxT_{HP}}} - F(\alpha,\beta)_{\mathrm{MaxT_{HP}}}$, $F(0, 0)$ being the RMS difference between the CTD salinity and the uncorrected tag salinity, and the suffix $\mathrm{MaxT_{HP}}$ indicates that F was calculated within ±50 m of the maximum T_{HP}. Thus, the effect of the correction is evaluated where the maximum thermal mass error is expected to be. A positive (negative) value of D indicates an improvement (degradation) of the data quality. Figure 3 presents a typical CTD and uncorrected and corrected tag profiles for each of the six experiments. The range of salinity error $F(0, 0)$ is large, varying between $O(10^{-3})$ and $O(10^{-2})$ g kg^{-1} depending on the experiment. In particular for the Boussole08 experiment, where the highest

TABLE 1. Salinity correction statistics per experiment: T_{HP}; error magnitude; values of α_{opt}, β_{opt} coefficients for each experiment; averaged magnitude for both the optimum and generic correction in terms of salinity and density, with standard deviation indicated in parentheses. The error and correction magnitude are calculated within ±50 m of the maximum T_{HP}.

Expt	Tags tested (No. of profiles)	Ascent speed ($m\ s^{-1}$)	Max temp gradient (°C s^{-1})	Max T_{HP} (°C)	α_{opt}, β_{opt} (averaged)	Salinity (±50 m of max T_{HP})			Density (±50 m of max T_{HP})		
						Error (g kg^{-1})	Optimum correction (g kg^{-1})	Generic correction (g kg^{-1})	Error (g kg^{-1})	Optimum correction (g kg^{-1})	Generic correction (g kg^{-1})
Albion09	7 (21)	1.0	0.06	0.67	0.009, 0.006	0.012	0.000 (0.002)	−0.002 (0.003)	0.010	0.000 (0.002)	−0.002 (0.002)
Albion08	5 (15)	0.75	0.08	0.83	0.009, 0.014	0.009	0.002 (0.002)	−0.003 (0.003)	0.008	0.002 (0.002)	−0.001 (0.003)
iStar14	16 (16)	1.0	0.11	−0.87	0.046, 0.088	0.023	0.001 (0.006)	0.001 (0.006)	0.019	0.001 (0.005)	0.001 (0.004)
Boussole09	3 (12)	0.35	0.13	1.10	0.062, 0.002	0.022	0.009 (0.011)	0.004 (0.002)	0.022	0.009 (0.006)	0.003 (0.001)
Carols09	7 (21)	1.3	0.18	1.78	0.014, 0.027	0.022	0.005 (0.011)	0.000 (0.021)	0.024	0.005 (0.010)	0.003 (0.017)
Boussole08	4 (28)	0.7	0.47	4.34	0.084, 0.077	0.053	0.033 (0.021)	0.026 (0.012)	0.073	0.036 (0.015)	0.021 (0.004)

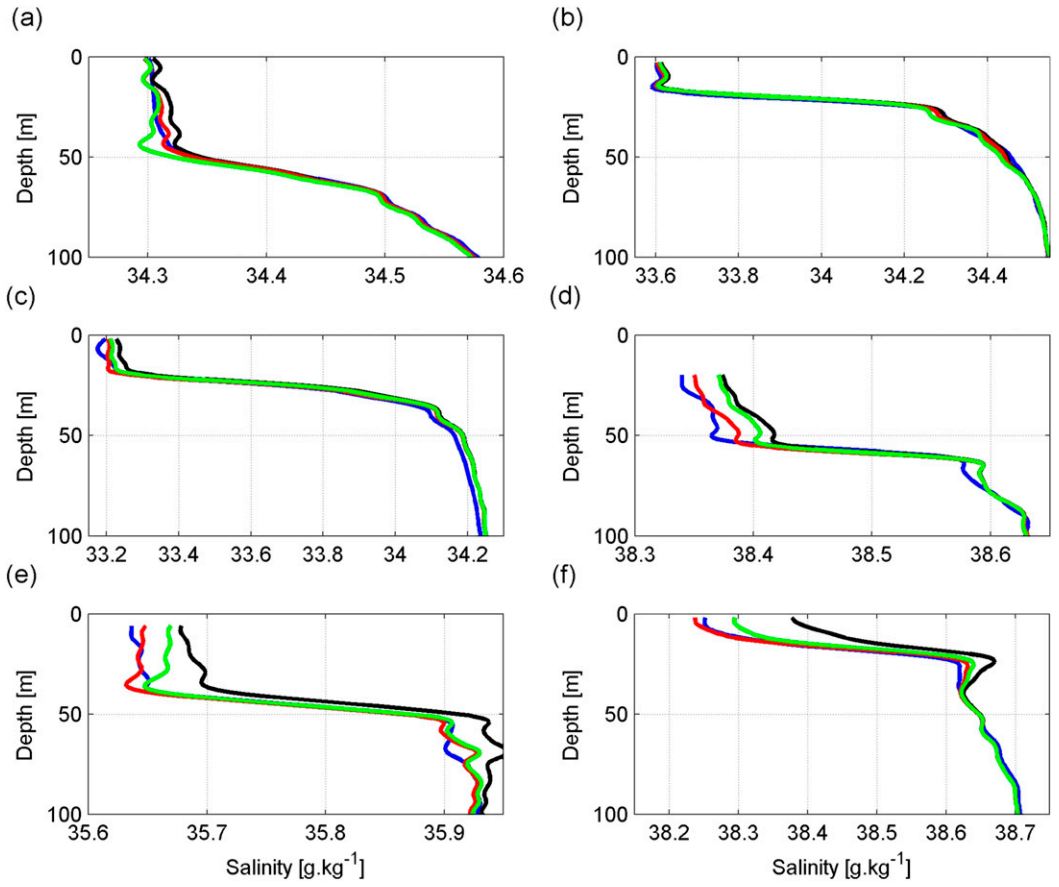

FIG. 3. Reference CTD and typical tag profiles for all six experiments: (a) Albion08, (b) Albion09, (c) iStar14, (d) Boussole09, (e) Carols08, and (f) Boussole08. The four curves in each panel represent the reference CTD profile (blue), noncorrected tag profile (black), tag profile corrected with a pair of optimum coefficients (red), and tag profile corrected with a pair of generic coefficients (green).

T_{HP} were encountered, the RMS error reaches values as high as 0.053 g kg^{-1} and the maximum error within a profile exceeds 0.1 g kg^{-1} (Fig. 3f). Conversely, the two Albion experiments, with their weaker temperature gradients and T_{HP}, exhibit the smallest RMS error (0.009 and 0.012 g kg^{-1}, respectively). Our results suggest that large discrepancies between the tag and CTD can be expected for T_{HP} values exceeding ~1°C (Table 1). These discrepancies are largely reduced for the three experiments presenting the highest T_{HP} values by the correction scheme of Eq. (4) used with optimally tuned coefficients, with a correction amounting to at least 25% and up to 62% of the original error. This implies that a large part of the error for high T_{HP} experiments is due to thermal mass and that it is effectively removed by the correction scheme adopted here. Conversely, the other three experiments see only a small error decrease, suggesting that most of their RMS difference is due to issues unrelated to thermal mass. In particular for the Albion08 and Albion09 experiments, the very low RMS difference and optimal correction value of $O(10^{-3})$ g kg^{-1} indicate that an RMS difference of ~0.01 g kg^{-1} represents a nearly irreducible error, considering the accuracy of the tag and CTD sensors. Note that following this optimal coefficient test, 9 out of the 113 profiles tested are found to show insignificant correction in spite of a large initial error. These large error profiles are assumed to be affected by nonthermal mass–related error and are excluded from analysis in subsequent sections.

3) OPTIMUM COEFFICIENT VALUES

The optimum coefficient values vary depending on the experiment, with the experiment averaged initial error α ranging between 0.9% and 8.4% and the relaxation time ($1/\beta$) ranging between 11 and 170 s. The reason for the particularly large range of values for the coefficients is unclear although all but one (Boussole09) experiment suggests that α and $1/\beta$ compensate for each other; that is, when the initial error is high (low), the relaxation time is short (long). This compensation between the two

coefficients is confirmed later [section 3b(3); Fig. 6] and likely causes a large range of coefficients to yield nearly equal corrections, hence the various values found in Table 1. In addition, the properties of the environment in which profiles are conducted could also be partly responsible for the coefficient values. To explore this possibility, we test the ability to predict the values of α and β from environmental predictors. First, coefficients optimized for each individual profiles following (5) are estimated, yielding 104 pairs of α_{ind} and β_{ind}. Then predicted values of α are fitted linearly with 10 environmental predictors obtained from each profile according to

$$\alpha_{pred}(n) = b_0 + b_1 X_1(i) + b_2 X_2(i) + \cdots + b_{10} X_{10}(i) + \varepsilon(i). \quad (6)$$

Here, the coefficients b_0–b_{10} are solved by minimizing the sum of residuals squared $\varepsilon(i)^2$. Terms X_1–X_{10} correspond to the 10 following environmental predictors: maximum T_{HP}, depth, and temperature of the maximum T_{HP}; and maximum, mean, and standard deviation of the temperature gradient, minimum, maximum, and mean temperature, and mixed layer thickness. A similar operation is conducted for β using the same environmental predictors. Results show that the predicted values α_{pred} and β_{pred} are linearly fitted with α_{ind} and β_{ind} with a coefficient of determination $R^2 = 0.57$ and $R^2 = 0.53$, respectively. However, if α_{ind} is added as X_{11} to determine β_{pred}, then the coefficient of determination becomes 0.91. Similarly, if β_{ind} becomes X_{11} in the determination of α_{pred}, the coefficient of determination for the latter becomes 0.92. This highlights the relative importance of the α–β compensation with regard to environmental properties in the profile. To summarize, while α and β compensate each other and an effective correction can be obtained from a large range of coefficient values [section 3b(3)], environmental properties may ultimately decide the best coefficient values within this large range of effective correction coefficients. Following these assumptions on the variability of the coefficients, it seems reasonable that a set of generic coefficients could yield sufficient correction for any kind of profiling environment.

b. *Generic correction coefficients*

1) Determination of coefficients

To determine a set of generic coefficients, we adapted the method delineated by (5), setting nc = 60. The nc includes 10 randomly chosen profiles from each of the six cruises, in order to avoid a bias generated by the different number of profiles tested during each experiment. This test is repeated 200 times, and we average these 200 pairs of α and β coefficients to obtain our generic coefficients. The coefficients obtained via this method are $\alpha_{gen} = 0.041$ and $\beta_{gen} = 0.060\ s^{-1}$, or an initial error of 4.1% and a relaxation time of ~17 s, respectively, and yield an average correction of $0.011\ g\,kg^{-1}$ out of an original averaged error of $0.035\ g\,kg^{-1}$.

2) Effects of the generic correction on salinity data

The set of generic coefficients performs particularly well for the Boussole08 dataset, which exhibits the strongest temperature gradient. In this case, around 50% of the error is resorbed through the use of generic coefficients, a figure that compares well with the ~60% error decrease obtained with the optimum coefficients. Aside from this experiment, the improvement brought by the generic coefficients is more modest but still significant when the initial discrepancy is high. The salinity data from Boussole09 are corrected by about 20% (Table 1) and while the average value of correction for the profiles of the Carols08 experiment is null, a large number of these profiles are well corrected by the generic coefficients (Fig. 3e). The high standard deviation for the correction of the Carols08 experiment demonstrates, however, that the changes brought to the profiles are unequal in quality depending on the tag it applies for. On the lower end of the salinity error range, the generic set of coefficient yields either insignificant improvement or, in the case of Albion08, a moderate degradation of the data. In this case, illustrated in Fig. 3a, the maximum discrepancy of $\sim 0.03\ g\,kg^{-1}$ is reached around the halocline at 45-m depth and indicates an overshoot of the correction. This overshoot is resorbed following the halocline as the tag and CTD profiles converge from ~40-m depth to the surface. Some profiles of the Carols08 experiment follow a similar pattern of degradation.

To further asses the performance of the generic coefficients on this dataset, the values of uncorrected and corrected salinity error—as defined in Table 1—for each individual profile are sorted according to their maximum T_{HP} and averaged per T_{HP} bins of 0.5°C. The results of this experiment, displayed in Fig. 4, demonstrate that the correction performance for T_{HP} values less than 2.0°C is null on average, and with a particularly low standard error. The RMS error increases sharply for the uncorrected data beyond this T_{HP} value, and it systematically exceeds $0.05\ g\,kg^{-1}$. The RMS error for the salinity corrected with the generic coefficient is strongly reduced, however, and for each T_{HP} bin, it generally becomes half the value of the original error. The results in Fig. 4 demonstrate that the correction applied with a

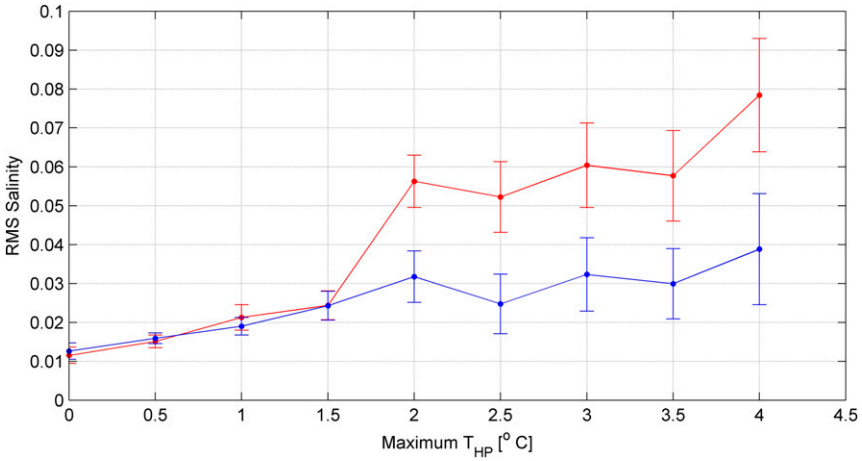

FIG. 4. RMS difference of reference and tag salinity as a function of T_{HP}, calculated from all the data points located within ±50 m of the maximum T_{HP} for the six experiments mentioned in this study. The red and blue lines represent the uncorrected and corrected data, respectively (using the set of generic coefficients). The standard error of the estimate (error bars) is indicated.

generic coefficient does not degrade the data when a correction may not be needed (very low T_{HP}) and significantly improves the data quality otherwise. Besides slightly degraded profiles, such as in Fig. 1a, a phenomenon independent of the correction performance may lead to an apparent degradation of the data in statistics of the two Albion experiments. Since high-frequency errors have been eliminated by the use of a 10-m low-pass filter prior to all our statistical tests, a likely cause could be a slight misalignment of the CTD and tag pressure sensors, or slight changes of positioning of the tags in between some of the casts. Such misalignment may lead to the temperature and salinity profiles being slightly offset, which could artificially cancel the effect of a small thermal mass error or conversely artificially inflate the error of properly corrected profiles. The case study in section 4 will enable the performance of the generic coefficients in a situation of low T_{HP} values to be more accurately evaluated.

3) IMPACT OF THE GENERIC CORRECTION ON THE DENSITY ERROR

To assess the potential contribution of uncorrected thermal lag errors of the temperature sensor on the density results, we estimate the values of RMS error for the raw and corrected density profiles (Table 1). For all but one experiment the density error (kg m^{-3}) is close to the salinity discrepancy (g kg^{-1}); therefore, it seems reasonable to assume that the salinity contribution to the density error largely dominates that of temperature. To confirm this assumption, the density error for each individual profile is converted to an equivalent salinity error after calculation of the coefficient of sensitivity of density to salinity, at fixed temperature and for a change of salinity of ±0.5 g kg^{-1}, $\Gamma_\rho = \partial\rho/\partial S_T$. This coefficient value is close to 0.77 for all the tags, which means that if salinity varies by 1 g kg^{-1}, then density will see a change of ~0.77 kg m^{-3}. The equivalent salinity error S_{Eq} is then obtained by dividing each profile density error by its Γ_ρ coefficient, and it is subsequently plotted against the actual salinity error RMS_S [which equals $F(0,0)_{MaxT_{HP}}$] in Fig. 5a. In this figure is also plotted a line of equation $y = (1/0.77)x$ that represents the value that should take S_{Eq} if it is entirely caused by RMS_S. Points located above (below) that line present a negative (positive) temperature error proportional to the vertical distance between the equivalent salinity error and the line. The results from this figure show that most of the points with a salinity error lesser than 0.03 g kg^{-1} fall very close to the y line, thus confirming that the temperature error has little significance in those cases. For errors larger than 0.03 g kg^{-1}, those profiles with T_{HP} values greater than ~2°C (largest dots in Fig. 5a) present a significant temperature error, as shown by the large vertical distance between the line and the dots in Fig. 5a. For each profile, the percentage of density error caused by temperature ε_T can be calculated from this vertical distance via

$$\varepsilon_T = \left(S_{Eq} - \frac{RMS_S}{\Gamma_\rho}\right)/S_{Eq}. \quad (7)$$

For each profile, the RMS density error and ε_T are used to obtain a value (kg m^{-3}) of density error caused by temperature E_T. Both E_T and ε_T are plotted against T_{HP} in Fig. 5c, and these results demonstrate that significant density error (as a result of temperature) can be

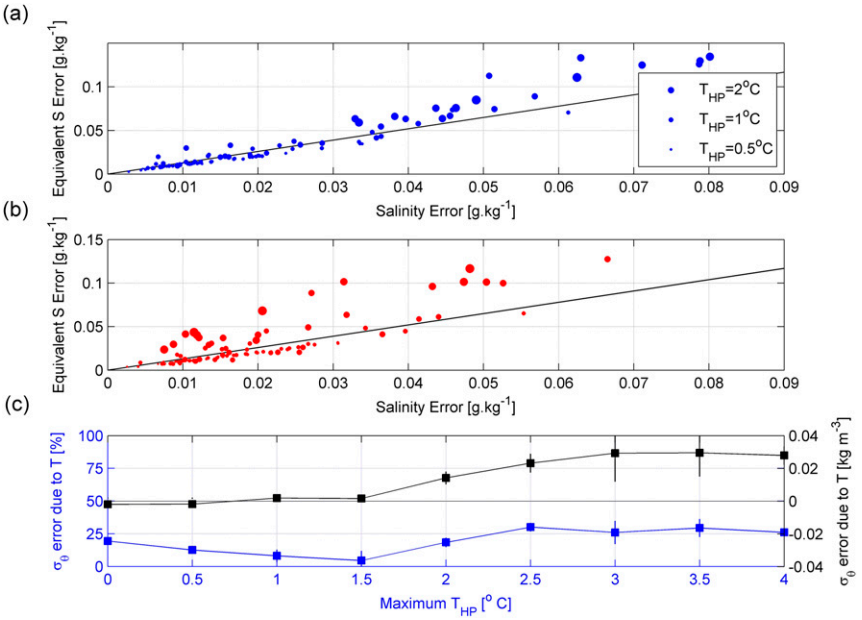

FIG. 5. Comparative plot of salinity error vs equivalent salinity error for each of the 104 profiles tested. (a) Errors for uncorrected tags and (b) errors for tags corrected with the set of generic coefficients. The size of the dots represents the magnitude of the maximum T_{HP} observed by each of the tags. The black line with a slope $a = 0.77$ represents the sensitivity of density to salinity, i.e., the change of density caused by a change of $1\,g\,kg^{-1}$ of salinity. The equivalent salinity error is calculated by converting density error into salinity error, with the assumption that the density error is entirely caused by a discrepancy in salinity. Data fulfilling this assumption will have their equivalent salinity error located on this line. (c) Density error caused by temperature expressed as a percentage of the total density error (blue) and as a value in kg m^{-3} (black), as a function of the maximum T_{HP}.

found only for profiles whose maximum T_{HP} values exceed 2°C, which corresponds to temperature gradients around 0.20°–0.28°C s^{-1}. In these cases E_T values greater than $0.01\,kg\,m^{-3}$ and amounting to ~20%–30% of the total density error are expected.

Results for the data corrected with the generic coefficients show a general decrease of the salinity and equivalent salinity errors, demonstrating that the correction scheme adopted here with a generic set of coefficient improves both salinity and density estimations. In those cases where E_T is large on the uncorrected profiles, the equivalent salinity error also decreases after correction as a result of the role of the salinity correction scheme, but the temperature-related errors remain essentially unchanged as can be seen from the large vertical distance between each dot and the y line (Fig. 5b).

4) GENERIC CORRECTION COEFFICIENT VALUES

Figure 6 displays the amount of correction for any pair of coefficients located within a large interval of α and β. The values of the generic set of coefficients ($\alpha_{gen} = 0.041$, $\beta_{gen} = 0.060\,s^{-1}$) and each optimum coefficient for individual profiles are also displayed in the figure. As shown in this graphic, a large beam exists—whose limits are defined by the $0.010\,g\,kg^{-1}$ isoline—within which pairs of coefficients yield a correction close to α_{gen}, β_{gen}. We can therefore assume that the generic coefficients will provide a correction close to the optimum correction for those profiles whose α_{ind}, β_{ind} are within the high-correction beam. This is the case for nearly half of the Boussole08 profiles and a third of the Carols09 profiles. This should also be the case for the Nakanowatari et al. (2017) experiment, where the pair of optimum coefficients ($\alpha_{Okh} = 0.05$, $\beta_{Okh} = 0.06\,s^{-1}$) was determined via a comparison of tag data and historical data from the *World Ocean Atlas 2013* (*WOA13*; Locarnini et al. 2013; Zweng et al. 2013) in the Okhotsk Sea, and yielded a decrease of salinity error of 0.07 psu over the uppermost 20 m of the water column. In contrast, those profiles whose α_{ind}, β_{ind} are located far from this beam will see the generic coefficients perform notably less well compared to the optimum correction. Note that contrary to the per-experiment statistics, the individual profile statistics show a trend where profiles with $T_{HP} < 2.0$°C (empty symbols in Fig. 6) are generally

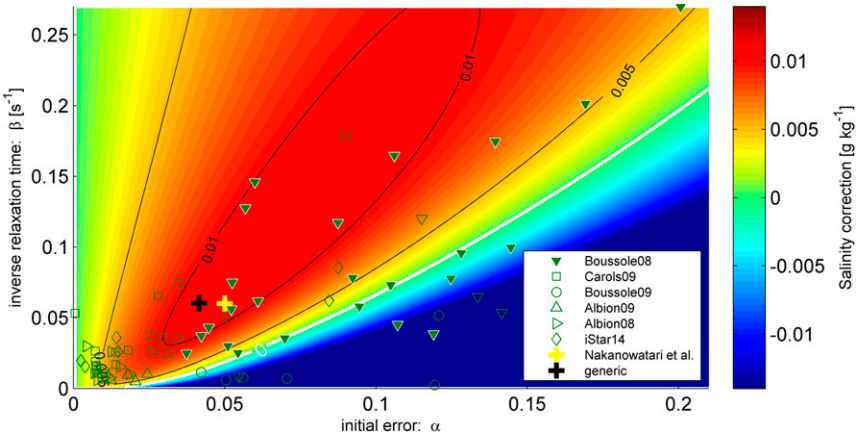

FIG. 6. Salinity correction for different values of coefficients α and β, with $F(\alpha, \beta)$ calculated within ±50 m of the maximum T_{HP} of all the casts tested. The limit of null correction (white isoline) and the values of optimum coefficients for each profile for all the experiments tested in this study, as well as from the experiment conducted by Nakanowatari et al. (2017) (symbols). Profiles whose maximum T_{HP} exceeds 2.0°C (filled symbols) and whose maximum T_{HP} fall below this limit (empty symbols).

corrected by small values of α and β, while profiles with large T_{HP} values and error tend to be corrected by large values of α and proportionally large values of β. Also, 26 profiles are located out of the figure limits, with nearly two dozen coefficient pairs of low T_{HP} profiles having a slightly negative value of α or β. This fact illustrates the difficulty in determining correction coefficients for very low T_{HP} conditions where little or no thermal mass error exists and where other errors might hamper the determination of coefficients. This issue is essentially solved when optimum coefficients are calculated per tag instead of individual profiles. While the variety of optimum coefficients should encourage users to determine their own optimum coefficients in the areas of deployment whenever possible, this is often not possible or ideal, as the seals may travel long distances throughout the deployment period and seasonal changes of water properties will also change the profiling environment. Our results have shown that the use of a set of generic coefficient provides satisfactory results for the conditions of the six aforementioned experiments, and the case study in the next section will further demonstrate the ability of this set of coefficients to provide an effective correction in operational conditions even when the T_{HP} is low.

4. Application of the generic correction to CTD-SRDL biologged data

a. Dataset

The thermal lag correction scheme described in (4) and with the generic coefficients ($\alpha_{gen} = 0.041, \beta_{gen} = 0.060\ s^{-1}$) is applied to five full-resolution CTD-SRDL tags deployed on southern elephant seals (SES) around the Kerguelen Islands in the Indian sector of the Southern Ocean during the austral summer. A unique dataset made of full-resolution CTD-SDRL hydrographic profiles acquired by five female SES from October 2014 to January 2015 has been used to test the robustness and efficiency of the thermal lag procedure and generic coefficients. Full-resolution tags record temperature, salinity, and pressure at a frequency of 0.5 Hz for every dive of the seal's journey. Besides the high resolution of this dataset, another advantage resides in the acquisition of both ascending and descending phases for every dive, which allows a comparison of the data and evaluation of the correction to be done. The environment in which the SES profiles were taken is marked by low temperatures and mild temperature gradients, successively negative between 0 and 150 m, then positive between 150 and 350 m (Fig. 7a). Accordingly, these weak temperature gradients are associated with weak T_{HP} values with the 20th–80th percentile envelope ranging between −0.17° and 0.22°C (Fig. 7c); this places this dataset below most of the T_{HP} values tested in the six experiments described earlier. Steady salinity changes occur throughout the water column.

b. Implementation of the correction

The thermal lag procedure was applied on the ascending and descending phases of every dive. A total of 22 308 dives ranging from depths of 150 m up to 1000 m have been used. The ascending phase of any

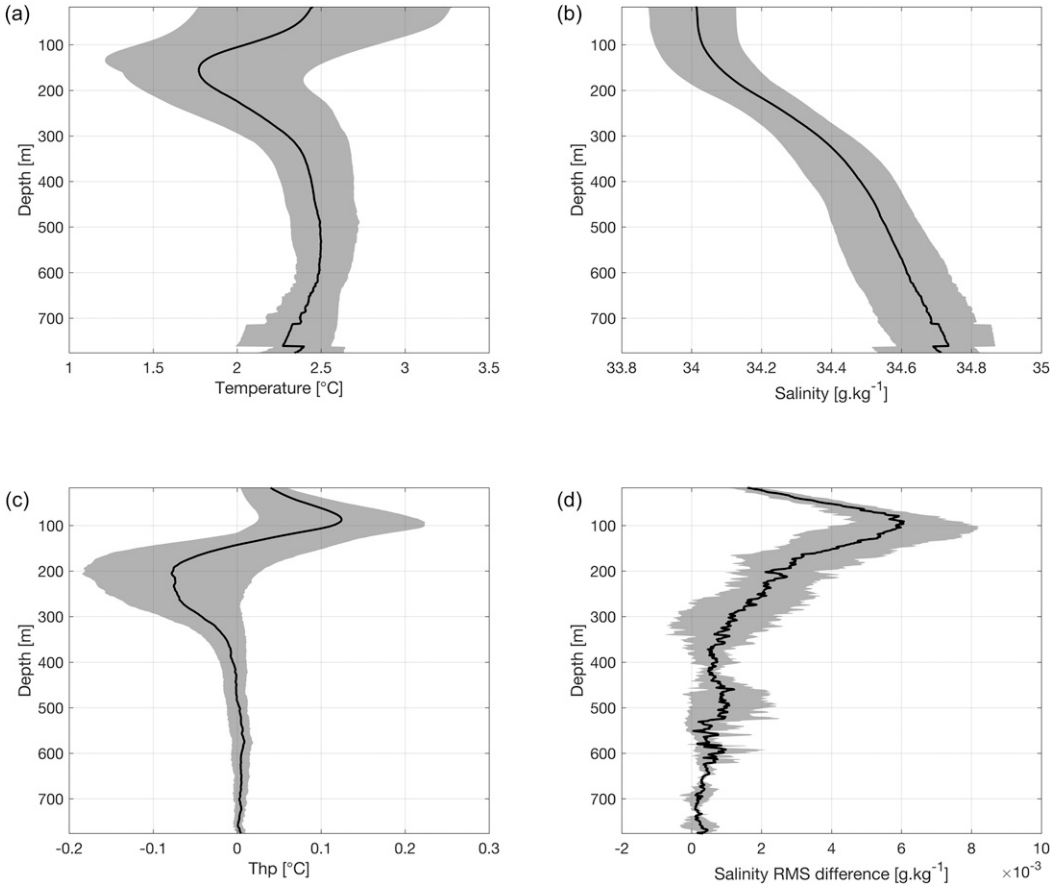

FIG. 7. (a) Mean temperature, (b) salinity, (c) T_{HP}, (d) $RMS_{ad\_raw} - RMS_{ad\_cor}$ profiles averaged for all full-resolution CTD-SRDL tags deployed on SES around the Kerguelen Islands. The shaded area envelopes represent the 20th and 80th percentiles in all four plots.

n dive is then compared to the descending phase of dive $n + 1$ for dives occurring within a 5-min interval in order to compare similar water masses. For each tag, the RMS error of ascent versus descent is first calculated at each depth z according to

$$\mathrm{RMS}_{\mathrm{ad}}(z) = \sqrt{\frac{1}{\mathrm{np}} \sum_{n=1}^{n=\mathrm{np}} [S_a(z,n) - S_d(z,n+1)]^2} \qquad (8)$$

where np is the total number of dives, and S_a and S_d are the salinity during ascent and descent, respectively. The term RMS_{ad} is calculated for both the uncorrected ($RMS_{ad_{raw}}$) and corrected ($RMS_{ad_{cor}}$) versions, and it shows values between ~0.02 and 0.03 g kg^{-1} for all but one tag (Table 2). These relatively large values are for the most part not caused by thermal lag and are likely related to slight changes in the geographic location of the ascent compared to the descent. The occurrence of a relatively large temperature RMS for all tags (Table 2) in spite of the weak temperature gradients confirms that environmental changes account for a large part of the RMS error. Therefore, the performance of the correction is evaluated through the difference of $RMS_{ad_{raw}}$ and $RMS_{ad_{cor}}$, with positive values indicating a decrease of the RMS error. All five tags see a significant improvement after the application of the thermal lag correction, where the difference between the ascending and descending phases for both the salinity and density field is minimized, as can be seen from the $RMS_{ad_{raw}} - RMS_{ad_{cor}}$ profile averaged for all tags (Fig. 7d). The impact of the thermal lag correction is more pronounced in the areas where stronger gradients of temperature are located, that is, between the surface and 300-m depth. The results obtained for this depth range are presented in Table 2. RMSs of salinity and potential density are the greatest for tag 35 because of some technical issues flagged with the salinity sensor of this particular tag and independent of the thermal lag procedure. This issue does not affect the values and

TABLE 2. Statistics for five tags deployed on SES in the Southern Ocean region off the Kerguelen Islands. Beside RMS_{ad_raw} and RMS_{ad_cor}, other variables include the RMS of temperature and the RMS of potential density. All RMS variables here have been calculated between the surface and 300-m depth.

Tag ID	No. of dives	RMS_T (°C)	RMS_{ad_raw} (g kg^{-1})	RMS_{ad_cor} (g kg^{-1})	RMS_{rho_raw} (kg m^{-3})	RMS_{rho_cor} (kg m^{-3})	Ascent velocity (m s^{-1})	Descent velocity (m s^{-1})
33	4689	0.122	0.033	0.028	0.027	0.022	−1.32	1.43
35	1536	0.122	0.086	0.084	0.077	0.075	−1.41	1.52
48	5739	0.103	0.025	0.022	0.020	0.017	−1.37	1.52
49	4950	0.081	0.021	0.018	0.017	0.014	−1.33	1.26
50	5394	0.065	0.020	0.016	0.017	0.013	−1.38	1.29

profile of $RMS_{ad_{raw}} - RMS_{ad_{cor}}$. Besides the averaged effect of the correction procedure over the water column presented in Fig. 7d, a typical pre- and post-correction profile is shown in Fig. 8. The profile that occurs in a region presenting sharper temperature variations sees its salinity difference between ascent and descent reduce by nearly 0.04 g kg^{-1}, which is a rather considerable improvement that is also reflected in the density profile (Fig. 8c) and in the temperature–salinity (TS) plan (Fig. 8d).

5. Summary and conclusions

The SRDL-CTD tag sensors are subject to the thermal mass phenomenon that affects other conductivity cells, such as the Sea-Bird Scientific SBE4. This paper

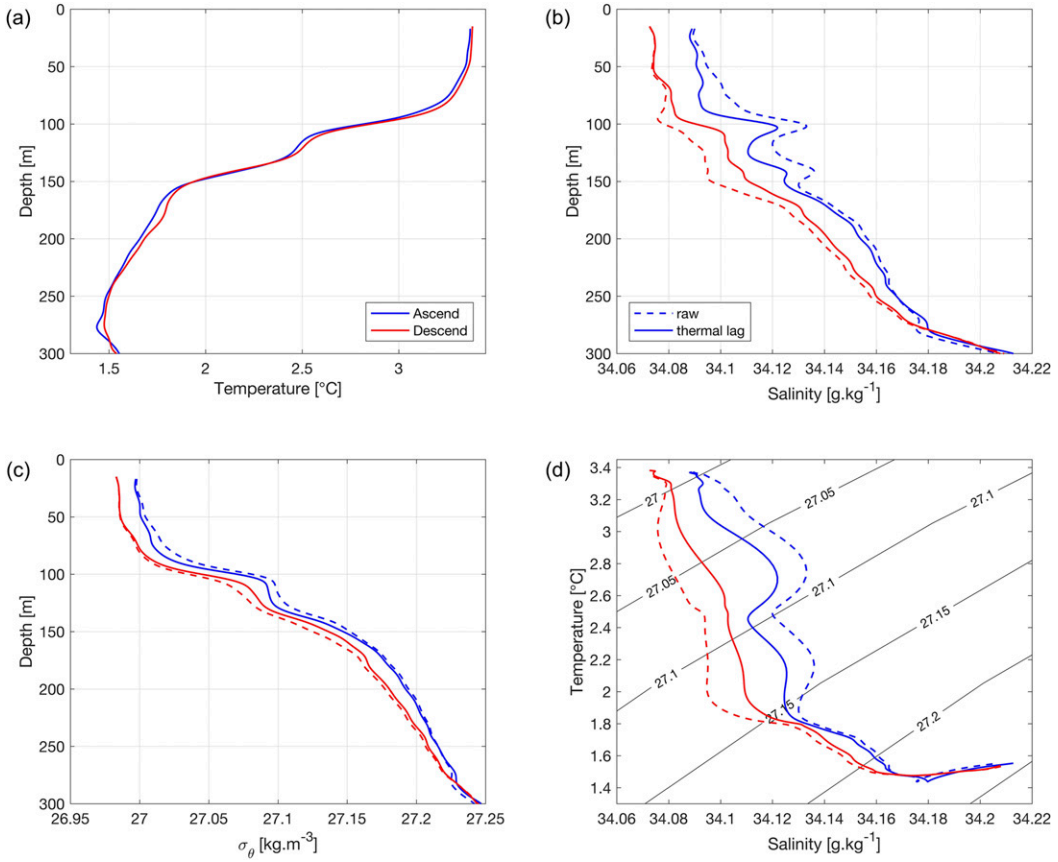

FIG. 8. A typical ascent (blue) and descent (red) profile comparison close-up view on the upper 300 m: (a) temperature, (b) salinity, (c) potential density, and (d) TS diagram. Raw profiles (dashed lines) and corrected profiles (solid lines) are marked in (a)–(c). To enhance visibility, a Gaussian filter with a 5-dbar window was applied to the profiles.

has documented the effect of thermal inertia on the tags' conductivity cell and provided evidence of thermal mass–induced errors increasing with the magnitude of the temperature gradient, and more specifically with the magnitude of the cumulated effect (T_{HP}) of the temperature gradient within a profile. The thermal mass applied on the conductivity cell reflects as a significant error in salinity estimates. Salinity error—defined here as the root-mean-square difference between a standard CTD upcast and a concurrent tag profile—amounting to $\sim 0.02\,g\,kg^{-1}$ for $T_{HP} < 2°C$, and $>0.05\,g\,kg^{-1}$ for larger T_{HP} occurs. A correction scheme was therefore developed to improve the salinity estimates. The main part of the correction methodology is a further development of the conductivity correction scheme of Lueck (1990), where correction coefficients represent the initial measurement error α and the inverse relaxation time β. However, the tag's temperature sensor is also affected by thermal mass, which implies that to obtain an accurate estimate of salinity, both the conductivity and temperature data are to be perfectly corrected simultaneously. For practical reasons described further in this section, this is difficult to achieve and thus we developed a correction algorithm to be applied directly to salinity. The correction algorithm is successfully implemented and tested on 42 different tags profiling in various hydrographic conditions and experiencing different ranges of temperature gradients, T_{HP}, and error. A comparison between tag and CTD profiles conducted simultaneously allowed to calibrate the coefficients α and β for each of the tags. These optimum coefficients systematically lead to a significant improvement for all tags whose T_{HP} is 2°C or above, with an error decrease of up to 60%. However, the range among which these optimal coefficients varies is large, suggesting a compensation effect between the magnitude of the initial error α and the relaxation time $1/\beta$, with possible further influence from the environment in which a given profile is conducted. A generic set of correction coefficients was therefore determined to account for the coefficients' variability. This set of coefficients ($\alpha_{gen} = 0.041$, $\beta_{gen} = 0.060\ s^{-1}$) yields an error decrease of nearly 50% for those profiles with a T_{HP} greater than 2°C (the latter that on average corresponds to temperature gradients of 0.20°–0.28°C s^{-1}). Results for lower T_{HP} or gradients were less clear because of intrinsic difficulties in evaluating small errors in CTD versus tag experiments. To further assess the performance of α_{gen} and β_{gen}, more than 22 000 profiles acquired from five different tags deployed in the Southern Ocean were evaluated. The difference in salinity between each downcast and upcast was used to assess the effectiveness of the generic coefficients, and was found to reduce the error on average by $0.006\,g\,kg^{-1}$ for profiles whose maximum T_{HP} was extremely low with averaged values of ~0.1°C. Those profiles presenting larger T_{HP} or temperature gradients saw very significant improvements with examples of upcast–downcast salinity difference reducing from 0.06 to $0.02\,g\,kg^{-1}$. Both this test and the CTD-versus-tags experiments demonstrate that the salinity correction leads to a substantial decrease of the density error.

Besides the effects of thermal mass on conductivity measurements/salinity estimates, temperature measurements also appear to be affected by thermal mass–induced errors. Temperature discrepancies are insignificant for $T_{HP} < 2°C$ but become large for $T_{HP} > 2°C$, amounting to ~25% of the error in density. While temperature gradients in excess of 0.20°–0.28°C s^{-1} (which is roughly equivalent to a T_{HP} of 2°C) are less frequently met in the ocean, they do still occur in some of the areas typically sampled by tag-equipped mammals (Nakanowatari et al. 2017) and call for an appropriate correction. However, the rather high limit above which the temperature error becomes significant (limit met by only 24 profiles) combined with a larger sensitivity of the least squares regression scheme used to determined correction coefficients make our dataset inadequate to define correction coefficients for temperature. Future development for the improvement of the temperature data requires a larger number of profiles acquired in high T_{HP} conditions as well as perfectly aligned pressure measurements for the tag and CTD used in the experiments.

Another possible improvement of the correction scheme could consist of adapting the correction coefficients according to the ascent velocity of the tag, as was done in Liu et al. (2015) for glider data. Different profiling speeds are expected to be met depending on the species or body condition of the mammals on which the tags are deployed, and these are likely to affect the value of the coefficients. However, as the results of Fig. 6 suggest, the range within which the correction yields similar results is large, allowing for performances of the generic coefficients to be satisfactory even when the profiling speed differs significantly from $\sim 1\,m\,s^{-1}$.

It is noteworthy that while the scheme described in this study applies directly to salinity data, the generic coefficients found here can be used to correct the conductivity following (1) and using $\alpha_C = -\alpha_{gen}$ and $\beta_c = \beta_{gen}$, following the assumptions developed in section 2c. A test has been conducted on the data from the six abovementioned experiments and yielded insignificant differences between the conductivity and salinity versions of the correction. It was, however, crucial to use the salinity to determine our coefficients in this study. The nature and relative magnitude of the

salinity error indeed made this determination more robust than using conductivity, whose signal and error are correlated with those of temperature. Last, while this paper documents the effects of our correction scheme on full-resolution tag data (1- or 0.5-Hz sampling rate), most of CTD-SRDL profiles available to date are heavily compressed because of satellite transmission constraints with a typical number of 20 data points per temperature/salinity profile (Boehme et al. 2009). The slow response nature of the thermal mass effect, and the low-pass filtering conducted on the data for the tags versus CTD test make it highly likely that the correction will be useful on low-resolution salinity data. Nakanowatari et al.'s (2017) work is an example of the successful implementation of this thermal mass correction algorithm on postprocessed low-resolution data in the Okhotsk Sea. Users are therefore encouraged to apply the thermal mass algorithm on their low-resolution salinity data, which should yield a significant reduction of the thermal mass–induced errors.

Acknowledgments. The present study is a contribution to the Observing System–Mammals as Samplers of the Ocean Environment (SO-MEMO) with funding and logistic support from CNES-TOSCA, IPEV, and CORIOLIS in situ ocean observation program. We are very grateful to D. Antoine for giving us access to the R/V *Tethys II* data, G. Reverdin for access to the R/V *Cotes de la Manche* data, and M.-N. Houssais for access to the R/V *L'astrolabe* data. The iStar14 data, obtained on the RSS *James Clark Ross* during the iSTAR JR294/295 cruise, were kindly made available to us by Karen Heywood and Helen Mallett. We also thank two anonymous reviewers for their constructive criticism. We extend our warm thanks to the crews and captains of the different research vessels.

APPENDIX

Equivalence between the Lueck and Picklo (1990) Recursive Filter and a Standard First-Order High-Pass Filter

Here it is shown that the recursive filter scheme devised by Lueck and Picklo (1990) to correct the thermal mass effect on a measured variable X (conductivity in their case) is formally equivalent to a standard first-order high-pass filter applied on the temperature discrete signal, once suitably rescaled.

The recursive filter of Lueck and Picklo (1990) is given by

$$X_T(n) = -bX_T(n-1) + \Gamma_X a[T(n) - T(n-1)], \quad \text{(A1)}$$

where X_T is the correction of conductivity added to the conductivity of the nth sample, T is the sample's temperature, n is the sample index, Γ_X is the sensitivity of X to temperature, and a and b are coefficients depending on α and β according to

$$a = \alpha/(1 + 0.25\beta f_n^{-1}) \quad \text{(A2)}$$

and

$$b = 1 - 2a\alpha^{-1}, \quad \text{(A3)}$$

where $f_n = (2\Delta_t)^{-1}$ is the Nyquist frequency function of the sampling interval Δ_t.

Define the high-pass filtered temperature signal T_{HF} as

$$T_{\mathrm{HP}}(n) = \frac{\tau}{\tau + \Delta_t}[T_{\mathrm{HP}}(n-1) + T(n) - T(n-1)], \quad \text{(A4)}$$

where τ is the time constant of the filter. Assuming that the correction is proportional to the high-pass filtered temperature signal, $X_T = AT_{\mathrm{HP}}$, and neglecting variations of the factor A between two consecutive samples (an excellent assumption in practice; see Fig. 2), a relation can be found between (A1) and (A4) providing the two identities $b = -\tau/(\tau + \Delta_t)$ and $A = \Gamma_X a(1 + \Delta_t/\tau)$. Using (A2) and (A3) and after some rearrangement, it comes that the recursive filter of Lueck and Picklo (1990) is strictly equivalent to rescaling the high-pass filtered temperature signal T_{HP} using a time constant $\tau = \beta^{-1} - 0.5\Delta_t$ and a factor $A = \Gamma_X\alpha(1 - 0.5\beta\Delta_t)^{-1}$.

Note that the filter is defined only if $\beta^{-1} > 0.5\Delta_t$ and that in the limit case $\beta\Delta_t \ll 1$, the time constant of the filter tends toward $\tau = \beta^{-1}$ and the correction simply tends toward $X_T = \Gamma_X\alpha T_{\mathrm{HP}}$.

REFERENCES

Antoine, D., and Coauthors, 2006: BOUSSOLE: A joint CNRS-INSU, ESA, CNES, and NASA ocean color calibration and validation activity. NASA GSFC Tech. Rep. NASA/TM–2006–214147, 68 pp., http://www.obs-vlfr.fr/Boussole/html/publications/pubs/BOUSSOLE_TM_214147.pdf.

——, P. Guevel, J.-F. Desté, G. Bécu, F. Louis, A. J. Scott, and P. Bardey, 2008: The "BOUSSOLE" buoy—A new transparent-to-swell taut mooring dedicated to marine optics: Design, tests, and performance at sea. *J. Atmos. Oceanic Technol.*, **25**, 968–989, https://doi.org/10.1175/2007JTECHO563.1.

Boehme, L., P. Lovell, M. Biuw, F. Roquet, J. Nicholson, S. E. Thorpe, M. P. Meredith, and M. Fedak, 2009: Technical Note: Animal-borne CTD-Satellite Relay Data Loggers for real-time oceanographic data collection. *Ocean Sci.*, **5**, 685–695, https://doi.org/10.5194/os-5-685-2009.

Garau, B., S. Ruiz, W. G. Zhang, A. Pascual, E. Heslop, J. Kerfoot, and J. Tintoré, 2011: Thermal lag correction on Slocum CTD

glider data. *J. Atmos. Oceanic Technol.*, **28**, 1065–1071, https://doi.org/10.1175/JTECH-D-10-05030.1.

Liu, Y., R. H. Weisberg, and C. Lembke, 2015: Glider salinity correction for unpumped CTD sensors across a sharp thermocline. *Coastal Ocean Observing Systems*, Y. Liu, H. Kerkering, and R. Weisberg, Eds., Academic Press, 305–325, https://doi.org/10.1016/B978-0-12-802022-7.00017-1.

Locarnini, R. A., and Coauthors, 2013: *Temperature*. Vol. 1, *World Ocean Atlas 2013*, NOAA Atlas NESDIS 73, 40 pp., http://data.nodc.noaa.gov/woa/WOA13/DOC/woa13_vol1.pdf.

Lueck, R. G., 1990: Thermal inertia of conductivity cells: Theory. *J. Atmos. Oceanic Technol.*, **7**, 741–755, https://doi.org/10.1175/1520-0426(1990)007<0741:TIOCCT>2.0.CO;2.

——, and J. J. Picklo, 1990: Thermal inertia of conductivity cells: Observations with a Sea-Bird cell. *J. Atmos. Oceanic Technol.*, **7**, 756–768, https://doi.org/10.1175/1520-0426(1990)007<0756:TIOCCO>2.0.CO;2.

McDougall, T., D. Jackett, F. Millero, R. Pawlowicz, and P. Barker, 2012: A global algorithm for estimating Absolute Salinity. *Ocean Sci.*, **8**, 1123–1134, https://doi.org/10.5194/os-8-1123-2012.

Mensah, V., M. Le Menn, and Y. Morel, 2009: Thermal mass correction for the evaluation of salinity. *J. Atmos. Oceanic Technol.*, **26**, 665–672, https://doi.org/10.1175/2008JTECHO612.1.

Morison, J., R. Andersen, N. Larson, E. D'Asaro, and T. Boyd, 1994: The correction for thermal-lag effects in Sea-Bird CTD data. *J. Atmos. Oceanic Technol.*, **11**, 1151–1164, https://doi.org/10.1175/1520-0426(1994)011<1151:TCFTLE>2.0.CO;2.

Nakanowatari, T., and Coauthors, 2017: Hydrographic observations by instrumented marine mammals in the Sea of Okhotsk. *Polar Sci.*, **13**, 56–65, https://doi.org/10.1016/j.polar.2017.06.001.

Roquet, F., J.-B. Charrassin, S. Marchand, L. Boehme, M. Fedak, G. Reverdin, and C. Guinet, 2011: Delayed-mode calibration of hydrographic data obtained from animal-borne satellite relay data loggers. *J. Atmos. Oceanic Technol.*, **28**, 787–801, https://doi.org/10.1175/2010JTECHO801.1.

——, and Coauthors, 2014: A Southern Indian Ocean database of hydrographic profiles obtained with instrumented elephant seals. *Sci. Data*, **1**, 140028, https://doi.org/10.1038/sdata.2014.28.

Treasure, A. M., and Coauthors, 2017: Marine mammals exploring the oceans pole to pole: A review of the MEOP consortium. *Oceanography*, **30**, 132–138, https://doi.org/10.5670/oceanog.2017.234.

Zweng, M., and Coauthors, 2013: *Salinity*. Vol. 2, *World Ocean Atlas 2013*, NOAA Atlas NESDIS 74, 39 pp., http://data.nodc.noaa.gov/woa/WOA13/DOC/woa13_vol2.pdf.